Available online at www.sciencedirect.com

SciVerse ScienceDirect

Ceramics International 38 (2012) 1085–1092

CERAMICS INTERNATIONAL

www.elsevier.com/locate/ceramint

Rietveld analysis of La^{3+}/Al^{3+} modified $PbTiO_3$ ceramics

Niranjan Sahu *, S. Panigrahi

Department of Physics, National Institute of Technology, Rourkela 769 008, Odisha, India

Received 30 April 2011; received in revised form 6 August 2011; accepted 19 August 2011
Available online 26 August 2011

Abstract

The polycrystalline samples of $(Pb_{0.70}La_{0.30})(Al_xTi_{1-x})O_3$ (PLAT) (x = 0.0, 0.05, 0.10, 0.15, 0.20) were synthesized by conventional solid-state reaction technique and annealed at two different temperatures. A single phase X-ray diffraction pattern was recorded with cubic symmetry of the space group $Pm-3m$.The Bragg–Brentano geometry is used for indexing, structural solution and Rietveld analysis for our powder samples. The detailed structural study was analyzed by employing Rietveld refinement techniques with the help of the Fullprof Program. The lattice parameters, cell volume, Wyckoff position of the atoms, bond lengths and angles have been calculated from the Rietveld analysis with the help of Powder Cell Program and by taking the refined parameter a stable crystal structure was suggested. It was observed that lattice parameter and cell volume decreases with increase of Al concentration. The crystallite size has been compared by three different methods: Scherrer's formula, Hall–Williamson method and Rietveld method. The scanning electron microscope (SEM) analysis of the samples shows the uniform microstructure with no abnormal grain growth and the grain size increases with annealing temperature and decreases with the increase of Al concentration. The elemental analysis was confirmed by energy dispersive spectrum analysis.

Keywords: B. Microstructure; D. Perovskite; Rietveld method; Crystallite size

1. Introduction

Lead titanate ($PbTiO_3$), which exhibits perovskites structure and a very high Curie temperature T_c = 490°, belongs to the most important ferroelectric and piezoelectric families [1]. The perovskite structure has been one of the most versatile structures for tailoring the properties of materials [2,3]. The perovskite structure forms the basis of several complex structures, which may be due to intergrowths, oxygen deficiency or due to cation ordering [4,5]. It has been shown that modification using aluminium, which occupies the B-sites, provides new structural defects, i.e. oxygen vacancies, during the sintering process [6]. Lead oxide also forms a liquid phase above its melting point (890 °C), which improves densification, but it also may affect the stoichiometry of the composition, due to its high volatility at the sintering temperatures. Therefore, an excess PbO is usually added to the initial raw materials, in order to prevent the deviation from the stoichiometry by lead loss and also to improve the densification, by forming the liquid phase. Lead titanate ($PbTiO_3$) has the perovskite (ABO_3) structure with the Pb atoms occupying the cell corners, Ti occupying the body canter, and the oxygen atoms sitting at the face centers. The cubic paraelectric phase has $Pm-3m$ symmetry, while the tetragonal ferroelectric phase has $P4mm$ symmetry [7]. Lead titanate $PbTiO_3$ (PT) and lead lanthanum titanate $Pb_{1-x}La_xTiO_3$ (PLT) are important perovskite ferroelectric materials which show remarkable ferroelectricity, piezoelectricity and pyroelectricity, because of their potential applications in the field of microelectronics and optoelectronics. The PT and PLT nanocrystals have been extensively studied in recent years [8–12]. The $PbTiO_3$ crystals show a para-ferroelectric phase transition at about 490 °C, transforming from the tetragonal to cubic phases. It is known that this transition is caused by the strain in the PT crystals with tetragonality c/a of 1.06. The ratio c/a in PT nanocrystals decreases with decreasing grain size [13]. The isomorphic substitution of lead with lanthanum gives rise to a decrease in the tetragonality, and the material with a formula of $Pb_{0.7}La_{0.3}TiO_3$ (PLT30) has a pseudo cubic perovskite structure [14].

Now a day, many studies have been carried out on the different synthesis methods, phase development, electric and

* Corresponding author. Tel.: +91 0661 2476518/2477001; fax: +91 0661 2472926/2471169.
E-mail addresses: nsahu76@gmail.com, nsahunitrkl@gmail.com (N. Sahu).

0272-8842/$36.00
doi:10.1016/j.ceramint.2011.08.035

dielectric behaviour of various perovskites structured ferroelectric ceramics, which can be applied to several micro and nano-electronic devices such as multilayer capacitors, microactuators and miniaturized transducers [15–17]. Aluminium as an acceptor ion may replace Ti^{4+} site and as addition segregates at grain boundaries [18]. Al belongs to valence stable ions; it can affect the stability of the material. It is also well known that the fluctuation of the oxidation state of the non metal ions (Al) results in the formation of oxygen ion vacancies to reserve the local electrical neutrality and causes thermally activated conduction [19].

Due to the above important facts we have prepared the $(Pb_{0.70}La_{0.30})(Al_xTi_{1-x})O_3$ (where $x = 0.0, 0.05, 0.10, 0.15$, and 0.20) by employing a solid state method at high temperature. In this paper, Rietveld analysis is used to refine structure and micro parameter of the PLTA material. Microstructural and elemental analysis was studied qualitatively.

2. Theoretical background

An accurate estimate of grain size/crystallite size becomes essential when such materials are produced with their crystallite size of the order of less than 100 nm.Though transmission electron microscope (TEM) is one of the powerful techniques for crystallite size measurement, it has certain limitations. Since TEM images represent only a local region, many samples and images are required to provide average information for the entire sample. Not only this, the TEM sample preparation method is an involved and a time consuming one. The XRD technique is free from these limitations.

X-ray diffraction is a simpler and easier approach for the determination of crystallite size of powder samples. The underlying principle of such a determination involves precise quantification of the broadening of the diffraction peaks. Based on this principle, a few techniques involving to calculate the crystallite size such as Scherrer equation, Hall–Williamson method and Rietveld method. The Scherrer's formulae can be written as [20],

$$S_C = \frac{\kappa\lambda}{\beta\cos\theta} \quad (1)$$

where constant 'κ' depends upon the shape of the crystallite size (= 0.89, assuming the circular grain), β = full width at half maximum (FWHM) of intensity vs. 2θ profile, λ is wavelength of the Cu Kα radiation (= 0.15418 nm) and θ is the Bragg's diffraction angle. The instrumental broadening factor has been taken into account during the FWHM calculation

$$(\beta = \sqrt{\beta_{obs}^2 - \beta_{ins}^2}).$$

According to Williamson–Hall (WH) method [21], the individual contributions to the broadening of reflections can be expressed as,

$$\beta\cos\theta = \frac{k\lambda}{S_C} + 4e\sin\theta \quad (2)$$

where $4e\sin\theta$ is the strain effect on the crystallites. It is mostly the correction of Scherrer's formula by taking into account of the strain. Using this equation one can calculate the average crystallite size and the strain of the samples.

A complete expression is used in the Rietveld method, which can be written as [22],

$$FWHM^2 = (U + D_{ST}^2)(\tan^2\theta) + V(\tan\theta) + W + \frac{IG}{\cos^2\theta} \quad (3)$$

where U, V and W are the usual peak shape parameters, IG is a measure of the isotropic size effect, D_{ST} = coefficient related to strain. IG and D_{ST} can be refined in Rietveld method.

3. Experimental details

The perovskite $(Pb_{0.70}La_{0.30})(Al_xTi_{1-x})O_3$ (where $x = 0.0$, 0.05, 0.10, 0.15, 0.20) ceramics have been prepared by the solid state method at high temperature. Stoichiometry ratios of PbO, La_2O_3, Al_2O_3 and TiO_2 with 99.9% purity were weighed using a high precision electronic balance. The above materials were mixed thoroughly with the help of agate mortar and pestle. The grinding was carried out under acetone till the acetone evaporates from the mortar. The mixture was ball milled for 8 h for homogeneous mixture and presintered at different temperatures with intermediate grindings. The samples were fired at 1000 °C for 6 h. The fine powders of the above compound were pressed into cylindrical pellets of 6 mm diameters and 1 mm thickness under a uni-axial pressure of 6 tons using a hydraulic press. Finally the pellets were sintered at 1150 °C for over 4 h with 5% extra lead oxide to compensate the lead loss at high temperatures [23] and then cooled to room temperature at the rate of 2 °C min^{-1}. All the above sintering processes were carried out in the air. The XRD patterns of all the samples were recorded using Philips PANalytical X'pert-MPD X-ray diffractometer (XRD) (Model-PW3020). The Cu Kα radiation was used as an X-ray source. The machine was operated at 35 kV and 30 mA. The data were collected with step size of 0.020 and time constant of 1 s. The scanning electron micrograph was recorded using a JEOL scanning electron microscope (SEM) (JEOL T-330) at room temperature. The compositional analysis was carried out by SEM-Energy dispersive spectroscopy (EDS).

4. Results and discussion

4.1. Structural analysis

Fig. 1 shows the XRD patterns of $(Pb_{0.70}La_{0.30})(Al_xTi_{1-x})O_3$ ($x = 0.0, 0.05, 0.10, 0.15, 0.20$) calcined at 1000 °C for 6 h. The lead titanate is a displacive type of ferroelectric compound having the tetragonal structure at room temperature, with very large distortion from a cubic structure [24]. We have observed that all the samples are in single-phase form could be indexed using $Pm-3m$ space groups with cubic symmetry.

Fig. 2 shows the X-ray diffraction patterns of $(Pb_{0.70}La_{0.30})(Al_xTi_{1-x})O_3$ ($x = 0.0$, 0.05, 0.10, 0.15, 0.20) sintered at 1150 °C for 4 h.The XRD patterns for all the

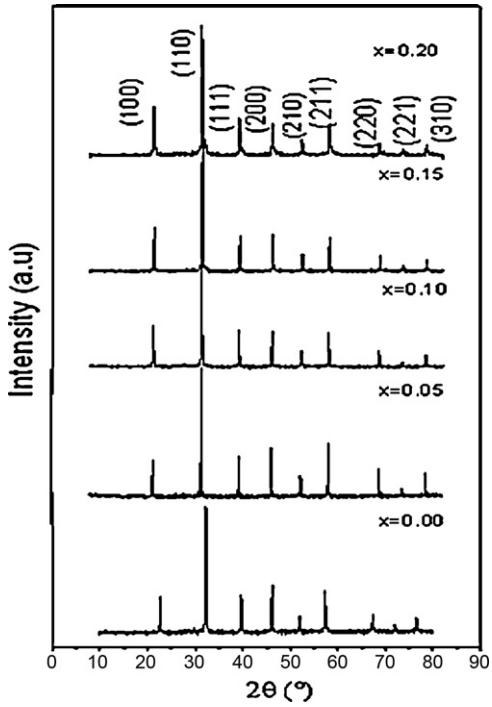

Fig. 1. XRD patterns of $(Pb_{0.70}La_{0.30})(Al_xTi_{1-x})O_3$ (where $x = 0.0, 0.05, 0.10, 0.15$, and 0.20) samples annealed at 1000 °C for 6 h.

samples were analyzed with the help of Fullprof program by employing Rietveld refinement techniques [25,26].The typical refined XRD pattern of 1000 °C for 6 h and annealed at 1150 °C for 4 h is shown in Figs. 3 and 4, respectively. We have observed that all the peaks could be well refined to the $Pm-3m$ space group. The average crystallite values calculated using Scherrer's formulae (Eq. (1)), Williamson–Hall (WH) method (Eq. (2)) and Rietveld method (Eq. (3)) are listed in Table 1 for both 1000 °C and 1150 °C annealed samples, respectively. One

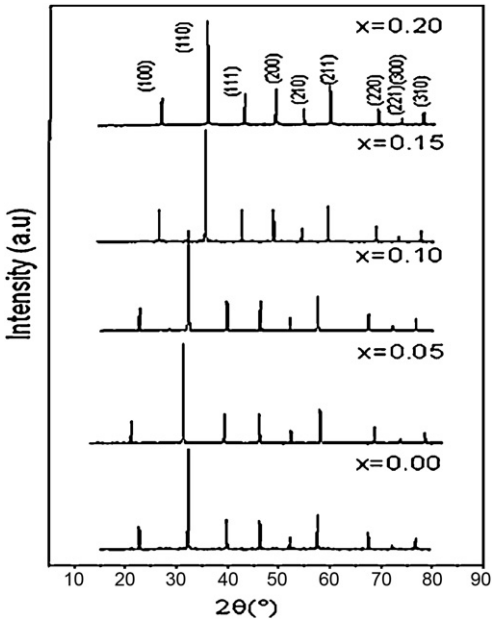

Fig. 2. XRD patterns of $(Pb_{0.70}La_{0.30})(Al_xTi_{1-x})O_3$ (where $x = 0.0, 0.05, 0.10, 0.15$, and 0.20) samples annealed at 1150 °C for 4 h.

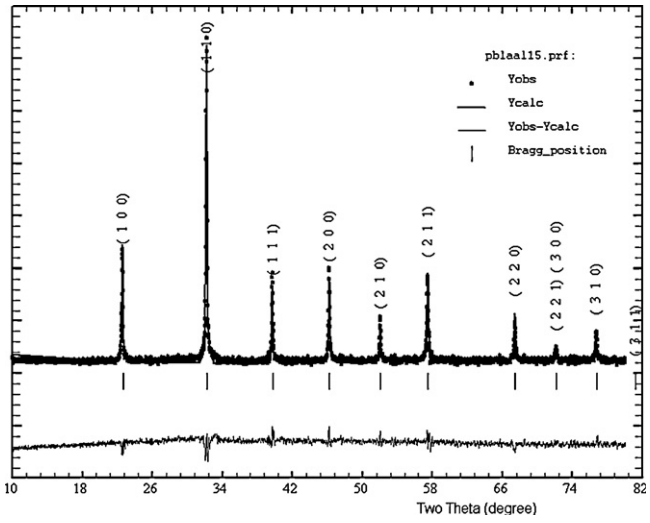

Fig. 3. Refined patterns in the typical sample $(Pb_{0.70}La_{0.30})(Al_{0.15}Ti_{0.85})O_3$ annealed at 1000 °C for 6 h with refined data obtained by the Rietveld method. The experimental points are given as a dot (•) and theoretical data is shown as solid lines. The difference between theoretical and experimental data is shown as a bottom line. The vertical lines represent the Bragg's allowed peaks.

can notice that the crystallite size obtained by Rietveld method is less than that of WH method. It is due to the correction of peak broadening factors taking into account of all instrumental factors. Also the crystallite size obtained by WH method is less than those obtained by Scherrer's formulae. It is because, the strain correction factor has been taken into account in case of WH method whereas it has not taken into account in Scherrer's method. The pseudo-Voight description of profile shape was determined as profile set up for Rietveld refinement. Refinement profile function value uses modern commercial Bragg–Brentano diffractometer and value of the sample broadening. Therefore, the Bragg–Brentano geometry is definitely the best

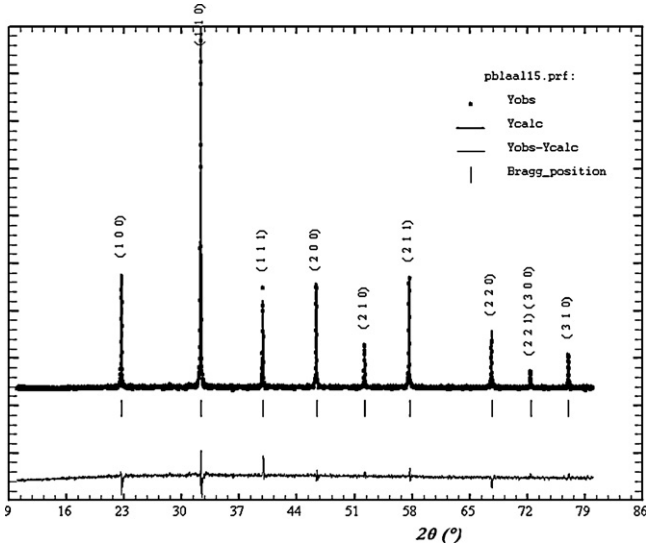

Fig. 4. Refined patterns in the typical sample $(Pb_{0.70}La_{0.30})(Al_{0.15}Ti_{0.85})O_3$ annealed at 1150 °C for 4 h with refined data obtained by the Rietveld method. The experimental points are given as a dot (•) and theoretical data is shown as solid lines. The difference between theoretical and experimental data is shown as a bottom line. The vertical lines represent the Bragg's allowed peaks.

Table 1
Crystallite size and Grain size of the sample $(Pb_{0.70}La_{0.30})(Ti_{1-x}Al_x)O_3$ (where x = 0.0, 0.05, 0.10, 0.15 and 0.20) samples annealed at 1000 °C for 6 h and 1150 °C for 4 h, respectively.

Sample composition	Crystallite size (nm)			Grain size (μm), SEM
	Scherrer method	WH method	Rietveld method	
$Pb_{0.70}La_{0.30}TiO_3$ (1000 °C)	21.2	19.7	18.6	1.24
$Pb_{0.70}La_{0.30}TiO_3$ (1150 °C)	38.6	37.8	36.3	4.26
$Pb_{0.70}La_{0.30}(Ti_{0.95}Al_{0.05})O_3$ (1000 °C)	20.4	18.9	18.1	1.13
$Pb_{0.70}La_{0.30}(Ti_{0.95}Al_{0.05})O_3$ (1150 °C)	37.7	37.0	36.1	4.20
$Pb_{0.70}La_{0.30}(Ti_{0.90}Al_{0.10})O_3$ (1000 °C)	20.0	18.3	17.2	1.12
$Pb_{0.70}La_{0.30}(Ti_{0.90}Al_{0.10})O_3$ (1150 °C)	36.4	35.9	35.2	4.12
$Pb_{0.70}La_{0.30}(Ti_{0.85}Al_{0.15})O_3$ (1000 °C)	19.6	17.4	16.4	1.05
$Pb_{0.70}La_{0.30}(Ti_{0.85}Al_{0.15})O_3$ (1150 °C)	34.8	34.1	33.0	4.03
$Pb_{0.70}La_{0.30}(Ti_{0.80}Al_{0.20})O_3$ (1000 °C)	18.5	17.1	15.7	1.02
$Pb_{0.70}La_{0.30}(Ti_{0.80}Al_{0.20})O_3$ (1150 °C)	33.9	33.0	32.1	3.98

choice for indexing, structure solution and Rietveld analysis of powder samples. The crystallite size plotted against different composition at different temperatures using these methods is shown in Fig. 5(a) and (b), respectively. It is observed that the average crystallite size increases with annealing temperatures and decreases with the increase in Al concentration. It is due to the formation of larger crystals at high temperatures. The crystallite size, lattice parameters, occupancy, fractional atomic positions, thermal parameters, etc. was taken as the free

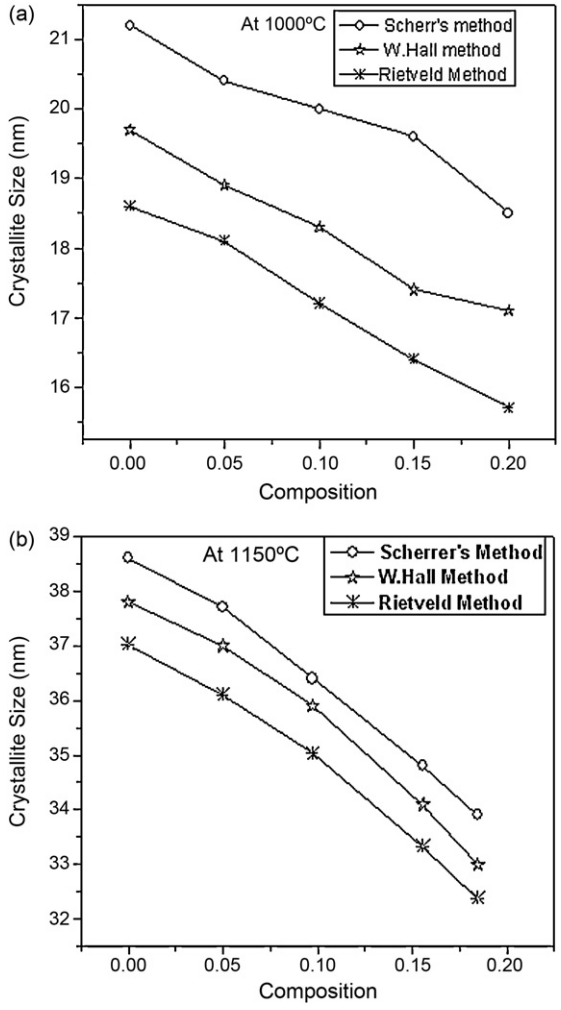

Fig. 5. (a) and (b) Compares the crystallite size verses composition using Scherrer's method, Williamson–Hall method and Rietveld method of $(Pb_{0.70}La_{0.30})(Ti_{1-x}Al_x)O_3$ (where x = 0.0, 0.05, 0.10, 0.15 and 0.20) samples annealed at 1000 °C for 6 h and 1150 °C for 4 h, respectively.

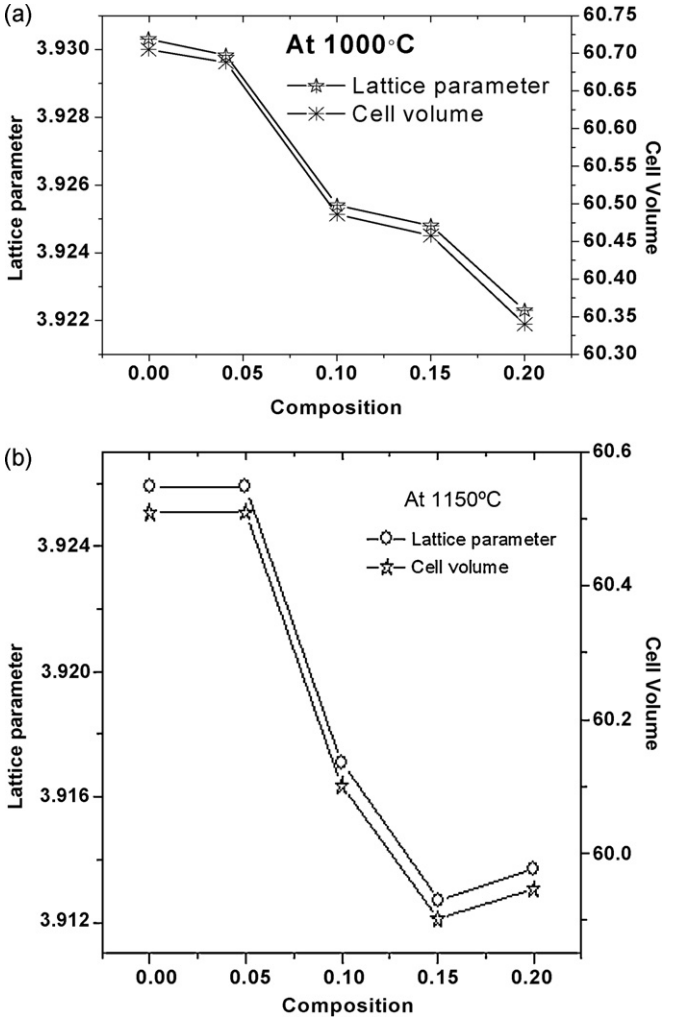

Fig. 6. (a) and (b) Lattice parameter, cell volume vs. compositions of $(Pb_{0.70}La_{0.30})(Ti_{1-x}Al_x)O_3$ (where x = 0.0, 0.05, 0.10, 0.15 and 0.20) samples annealed at 1000 °C for 6 h and 1150 °C for 4 h, respectively.

Table 2
Parameters obtained from Rietveld analysis of $(Pb_{0.70}La_{0.30})(Ti_{1-x}Al_x)O_3$ (where $x = 0.0, 0.05, 0.10, 0.15, 0.20$) samples annealed at 1000 °C for 6 h.

Parameters	Samples				
	$x = 0.00$	$x = 0.05$	$x = 0.10$	$x = 0.15$	$x = 0.20$
Space group	$Pm-3m$	$Pm-3m$	$Pm-3m$	$Pm-3m$	$Pm-3m$
Pb (Occup.)	0.633(8)	0.631(7)	0.682(2)	0.674(3)	0.665(4)
La (Occup.)	0.233(8)	0.231(8)	0.282(4)	0.270(7)	0.265(7)
Ti (Occup.)	0.995(7)	0.950(8)	0.906(5)	0.849(7)	0.807(8)
Al (Occup.)	–	0.051(8)	0.106(5)	0.158(3)	0.198(10)
$a = b$ (Å)	3.930(2)	3.929(9)	3.925(12)	3.924(19)	3.922(8)
C (Å)	3.930(2)	3.929(9)	3.925(2)	3.924(19)	3.922(8)
Volume (Å^3)	60.704(1)	60.688(11)	60.486(6)	60.457(6)	60.341(4)
χ^2 (chi^2)	2.12	1.74	1.40	1.88	1.73
R_p	11.9	20.2	16.9	21.0	23.2
R_{wp}	21.8	22.1	18.3	22.7	20.5
R_{Bragg}	13.0	14.3	10.8	11.7	12.2
R_f	8.52	12.9	8.8	10.7	13.3
R_{exp}	9.56	13.6	9.79	10.2	10.3
Pb–Ti/La (Å)	3.30(2)	3.41(4)	3.13(3)	3.05(2)	3.01(1)
Pb–Al–La (Å)	–	3.29(1)	3.35(2)	4.10(1)	4.23(2)
Ti/La–O1 (Å)	1.48(5)	1.88(8)	1.78(7)	1.77(7)	1.75(8)
Ti/La–O2 (Å)	2.21(5)	2.20(5)	1.95(9)	1.88(11)	1.80(5)
∠Pb–Ti/La–Pb	16.85(2)	18.28(3)	17.68(9)	16.77(7)	16.38(8)
∠Pb–Ti/Al–O1	102.32(5)	124.21(6)	118.14(7)	115.54(5)	113.24(5)
∠Pb–Ti/La–O2	45.51(3)	114.75(4)	110.43(2)	109.12(5)	105.82(5)
∠Pb–La–Al	–	105.52(1)	101.98(6)	101.78(5)	100.85(4)
∠La–O2–Al	–	121.41(2)	115.25(4)	111.56(4)	109.78(5)
∠La–O1–Al	–	104.45(1)	101.85(7)	100.81(2)	98.88(5)

parameter during the fitting. All the refined parameters, position of occupancies, bond lengths, bond angles calculated from the refined parameters and other parameters are listed in Tables 2 and 3 for the sample annealed at 1000 °C and 1150 °C, respectively. The site occupancy factors for each atom was refined separately and then fixed at the refined value. In the final refinement, the isotropic thermal parameters and the oxygen occupancy factor were refined. The lattice parameters and unit

Table 3
Parameters obtained from Rietveld analysis of $(Pb_{0.70}La_{0.30})(Ti_{1-x}Al_x)O_3$ (where $x = 0.0, 0.05, 0.10, 0.15$ and 0.20) samples annealed at 1150 °C for 4 h.

Parameters	Samples				
	$x = 0.00$	$x = 0.05$	$x = 0.10$	$x = 0.15$	$x = 0.20$
Space group	$Pm-3m$	$Pm-3m$	$Pm-3m$	$Pm-3m$	$Pm-3m$
Pb (Occup.)	0.633(8)	0.627(3)	0.646(7)	0.660(7)	0.629(3)
La (Occup.)	0.238(8)	0.279(3)	0.288(1)	0.263(3)	0.275(5)
Ti (Occup.)	0.995(7)	0.957(1)	0.895(5)	0.845(7)	0.806(9)
Al (Occup.)	–	0.054(7)	0.107(8)	0.158(9)	0.204(1)
$a = b$ (Å)	3.927(2)	3.925(6)	3.917(3)	3.912(7)	3.913(3)
C (Å)	3.927(2)	3.925(6)	3.917(3)	3.912(7)	3.913(3)
Volume (Å^3)	60.509(3)	60.508(6)	60.101(4)	59.909(2)	59.906(8)
χ^2 (chi^2)	2.12	2.32	2.34	2.35	2.38
R_p	19.9	19.3	16.1	10.6	10.3
R_{wp}	21.8	22.1	24.4	17.6	17.2
R_{Bragg}	13.0	13.1	11.8	8.45	15.7
R_f	8.52	11.9	7.13	7.08	13.5
R_{exp}	9.56	8.33	8.26	7.89	8.65
Pb–Ti/La (Å)	3.20(7)	3.56(8)	3.42(5)	3.32(5)	3.209(1)
Pb–Al–La (Å)	–	4.81(5)	3.98(4)	3.85(1)	3.54(1)
Ti/La–O1 (Å)	1.55(4)	1.89(4)	1.74(1)	1.71(2)	1.68(4)
Ti/La–O2 (Å)	2.04(2)	2.40(4)	2.12(4)	1.94(4)	1.81(2)
∠Pb–Ti/La–Pb	15.85(7)	19.21(4)	18.67(8)	17.54(5)	16.51(4)
∠Pb–Ti/La–O1	101.0(1)	112.29(4)	108.76(4)	105.25(5)	104.38(6)
∠Pb–Ti/La–O2	47.41(3)	113.93(4)	111.32(9)	110.23(5)	110.16(5)
∠Pb–La–Al	–	121.29(1)	120.56(2)	120.30(2)	119.95(6)
∠La–O2–Al	–	117.58(7)	114.32(4)	111.97(5)	110.84(4)
∠La–O1–Al	–	87.23(6)	84.52(1)	82.96(7)	80.52(7)

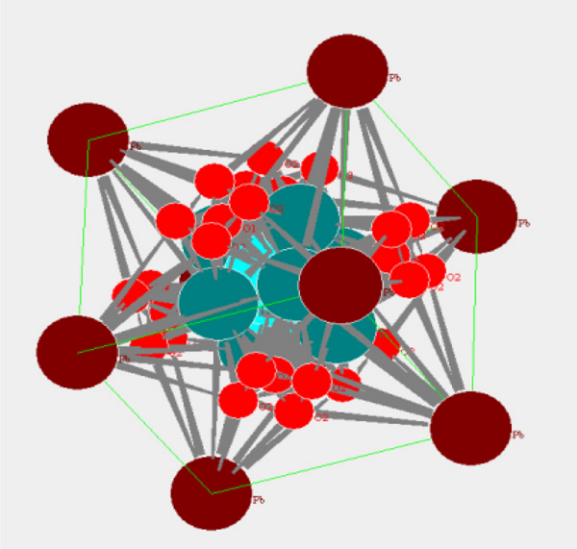

Fig. 7. Stable crystal structure using the refined parameters of the typical $(Pb_{0.70}La_{0.30})(Ti_{0.85}Al_{0.15})O_3$ samples annealed at 1150 °C for 4 h, respectively.

cell volumes are found to be decreased with the increase of Al concentrations, it could be due to the smaller ionic size of Al^{3+} (0.51 Å) to that of ionic size of Ti^{4+} (0.95 Å). Since Al does not have bonding d-orbit or d-electrons and the substitution of Al^{3+} for Ti^{4+} in $(Pb_{0.70}La_{0.30})(Al_xTi_{1-x})O_3$ is aliovalent, the effect of Al on the structure is quite different from the other substitutions of the PLT. From bond lengths it is confirmed that Al-doping reinforced the Co-valance of Pb–O, Which indicated that the Pb–O hybridization was strengthened [27]. The Rietveld refinement treatment was done to reduce the overlapping position in the same place between the Ti and Al. Therefore, the crystal structure becomes more stable. From this stable structure it is observed that crystal structure analysis is an important step to get high quality PLAT materials for microelectronics and optoelectronics applications. The lattice parameter and cell volume verses compositions for different annealing temperatures are shown in Fig. 6(a) and (b), respectively. Using the refined parameter the stable crystal structure was suggested, which is shown in Fig. 7. In crystallography a Wyckoff position is a point belonging to a set of points for which site symmetry groups are conjugate subgroups of the space group. Wyckoff positions are used in calculations of crystal properties. The splitting of the Wyckoff position of the atoms for all the compositions after refinement is capitalized in Table 4.

Table 4
The splitting of Wyckoff positions after refinement of $(Pb_{0.70}La_{0.30})(Ti_{1-x}Al_x)O_3$ (where $x = 0.0$, 0.05, 0.10, 0.15 and 0.20) samples annealed at 1150 °C for 4 h.

Wyckoff position of atoms	Samples				
	$x = 0.0$	$x = 0.05$	$x = 0.10$	$x = 0.15$	$x = 0.20$
Pb	1a	1a	1a	1a	1a
La	6b	6b	6b	6b	6b
Ti	8c	8c	8c	8c	8c
Al	6d	8d	1d	1d	1d
O	12e	6e	6e	6e	6e

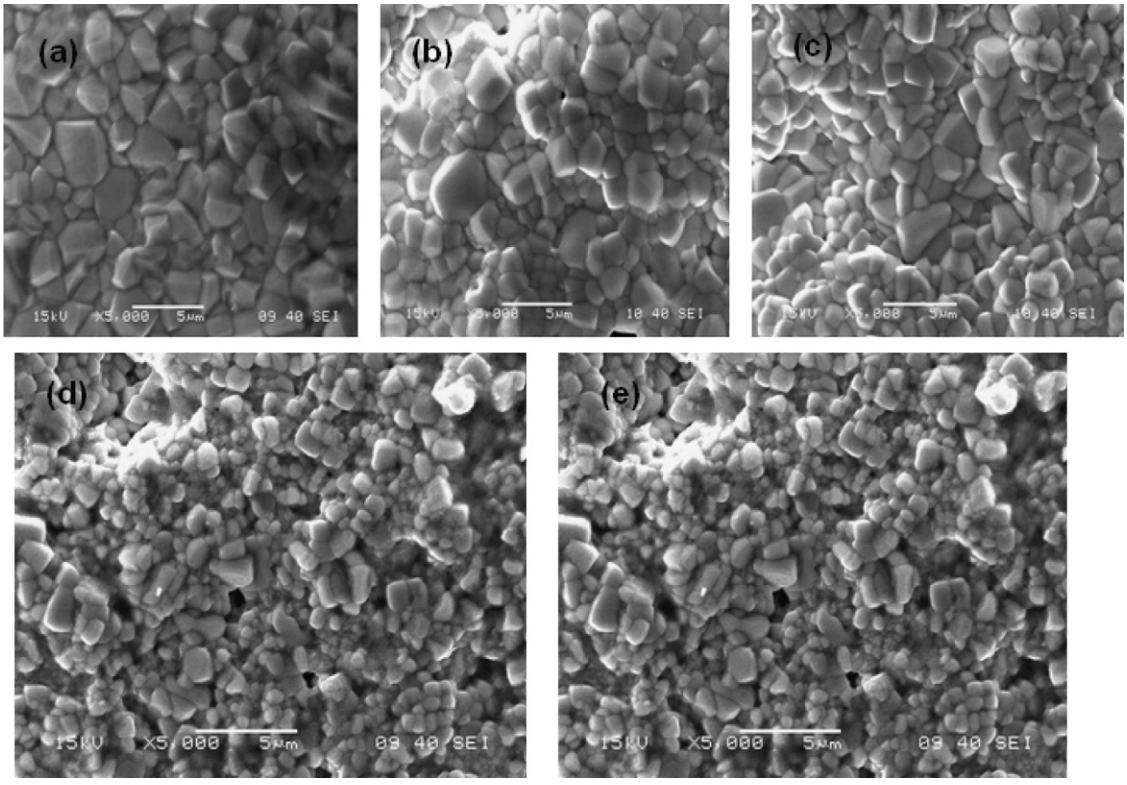

Fig. 8. (a–e) Scanning electron micrograph of $(Pb_{0.70}La_{0.30})(Ti_{1-x}Al_x)O_3$ (where $x = 0.0$, 0.05, 0.10, 0.15 and 0.20) samples annealed at 1150 °C for 4 h.

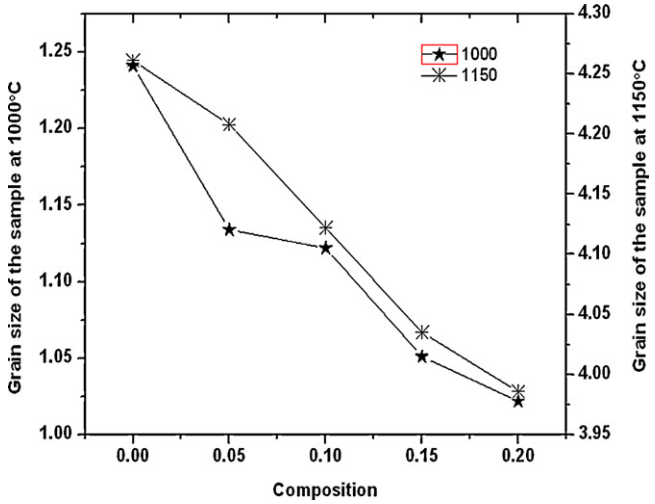

Fig. 9. Evolution of the grain size as a function of La concentration of the sample annealed at 1000 °C for 6 h and 1150 °C for 4 h, respectively.

4.2. Microstructural and elemental analysis

Fig. 8(a–e) exhibits the scanning electron micrographs of the $(Pb_{0.70}La_{0.30})(Ti_{1-x}Mn_x)O_3$ (where $x = 0.0$, 0.05, 0.10, 0.15, 0.20, 0.25) samples annealed at 1150 °C for 4 h, respectively. The micrographs indicate the existence of polycrystalline microstructure. The grains of equal sizes appear to be distributed homogeneously throughout the surface of the samples. One can notice the samples are uniform and the grains are in order of micron size. The average grain size of the sample is found to be 1.02–4.26 μm and there is uniform grain growth, which is desirable for getting better electrical and electrochemical properties. The variation of average grain size for all the samples with an increase in Al concentration with sintering temperature is listed in Table 1 and it was found that grain size decreases with increase of Al concentration. Generally Pb evaporates during the high temperature annealing. These micrographs revealed that

Table 5
Elemental analysis of $(Pb_{0.70}La_{0.30})$ $(Ti_{1-x}Al_x)O_3$ (where $x = 0.0$, 0.05, 0.10, 0.15 and 0.20) samples annealed at 1150 °C for 4 h.

Composition	Element	EDS (wt%)	Theoretical (wt%)
$x = 0.00$	Pb	47.29	47.34
	La	26.52	26.53
	Ti	16.28	16.31
	O	9.91	9.81
	Al	0	0.0
$x = 0.05$	Pb	45.92	45.96
	La	25.74	25.75
	Ti	15.03	15.04
	O	9.50	9.53
	Al	3.81	3.71
$x = 0.10$	Pb	44.35	44.65
	La	24.89	25.02
	Ti	14.00	13.85
	O	10.55	9.25
	Al	7.21	7.22
$x = 0.15$	Pb	43.39	43.42
	La	24.65	24.32
	Ti	12.69	12.71
	O	9.05	9.01
	Al	10.22	10.53
$x = 0.20$	Pb	42.22	42.25
	La	23.66	23.67
	Ti	11.62	11.64
	O	8.85	8.76
	Al	13.65	13.67

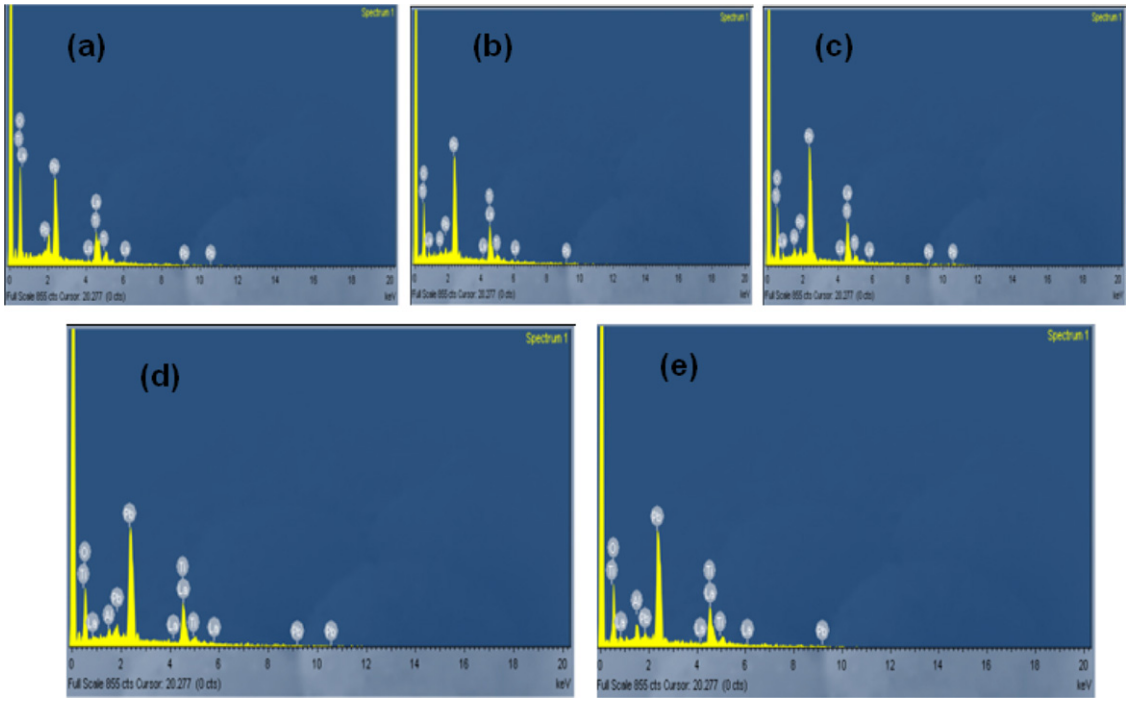

Fig. 10. (a–e) Energy dispersive spectrum of $(Pb_{0.70}La_{0.30})(Ti_{1-x}Al_x)O_3$ (where $x = 0.0$, 0.05, 0.10, 0.15 and 0.20) samples annealed at 1150 °C for 4 h.

the grain structure of the samples is dense, crack free, smooth having an apparent uniform thickness. Further these micrographs revealed that the increased grain size is due to the increasing of sintering temperature. Fig. 9 shows the grain size verses compositions at different annealing temperatures.

The energy dispersive spectrum (EDS) analysis reveals that, all the compositions present in the samples are as prepared. The SEM-EDS is shown in Fig. 10(a–e), respectively. This figure clears the EDS analysis of all the doping concentration; the theoretical wt% of the elements is more or less the same with the wt% calculated from the EDS spectra, which shows a consistency of the elemental wt% present in the green ceramics. The relation between the theoretical wt% and EDS spectra wt% of different elements of various compositions of $Pb_{0.70}La_{0.30}Al_xTi_{1-x}O_3$ ceramics is given in Table 5. It is observed that both the wt% is more or less the same with a little variation.

5. Conclusions

A structural study was performed on Al doped $(Pb_{0.70}La_{0.30})(Ti_{1-x}Al_x)O_3$ ($x = 0.0, 0.05, 0.10, 0.15, 0.20$) compounds prepared by the conventional solid state reaction technique. The formation of the perovskite structure has been confirmed from X-ray diffraction study. The lattice parameter (which determine the positions of the reflections) and cell volume decreases with increase of Al concentration. The Rietveld refinement method was undertaken for crystallite size estimation and structural information from powder samples. The treatment was done to reduce the overlap position in the same place between the Ti and Al. The Rietveld analysis suggests that the Goodness of fitting parameters, bond lengths and angles are useful for the development of the perovskites structure of the materials, using the refined parameter a stable crystal structure is suggested. The SEM micrographs revealed, increased grain size with the increase in sintering temperature and decreases with the increase of Al concentration. By elemental analysis we confirmed that the sample is as prepared.

Acknowledgements

All the experimental works have been carried out using the facilities available at National Institute of Technology Rourkela, Odisha, India. Authors are thankful to the Head, Ceramic and Metallurgy and Material Science Engineering Department, NIT, Rourkela, for XRD and SEM-EDS measurements.

References

[1] B. Jaffe, W.R. Cook, H. Jaffe, Piezoelectric Ceramics, Academic Press, New York, 1971.
[2] G.H. Haertling, Ferroelectric ceramics: history and technology, J. Am. Ceram. Soc. 82 (1999) 797–818.
[3] A.J. Moulson, J.M. Herbert, Electroceramic, 2nd ed., Wiley, Chichester, 2003.
[4] T. Takahashi, Lead titanate ceramics with large piezoelectric anisotropy and their applications, Am. Ceram. Soc. Bull. 69 (1990) 691–695.
[5] L.E. Cross, Review ferroelectric materials for electromechanical transducer applications, Mater. Chem. Phys. 43 (1996) 108–115.
[6] G. Shirane, S. Hoshino, On the phase transition in lead titanate, J. Phys. Soc. Jpn. 6 (1951) 265–270.
[7] G. Shirane, R. Pepinsky, B.C. Frazer, X-ray and neutron diffraction study of ferroelectric $PbTiO_3$, Acta Crystallogr. 9 (1956) 131–140.
[8] B. Noheda, D.E. Cox, G. Shirane, R. Guo, B. Jones, L.E. Cross, Stability of the monoclinic phase in the ferroelectric perovskite $PbZr_{1-x}Ti_xO_3$, Phys. Rev. B 63 (2001) 14103–14112.
[9] A. Dutta, T.P. Sinha, S. Shannigrahi, Dielectric relaxation and electronic structure of $Ca(Fe_{1/2}Sb_{1/2})O_3$, Phys. Rev. B 76 (2007) 155113.
[10] N. Ortega, A. Kumar, P. Bhattacharya, S.B. Majumder, R.S. Katiyar, Impedance spectroscopy studies of the $Pb(Zr,Ti)O_3$–$CoFe_2O_4$ multilayers thin films, Phys. Rev. B 77 (2008) 014111.
[11] T. Ohno, D. Suzuki, K. Ishikawa, H. Suzuki, Size effect for lead zirconate titanate nano-particles with PZT (40/60) composition, Adv. Powder Technol. 18 (2007) 579–589.
[12] K. Ishikawa, T. Uemori, Surface relaxation in ferroelectric perovskites, Phys. Rev. B 60 (1999) 11841–11845.
[13] S.K. Mishra, D. Pandey, A.P. Singh, Effect of phase coexistence at LT morphotropic phase boundary on the properties of $Pb(Zr_xTi_{1-x})O_3$ ceramics, Appl. Phys. Lett. 69 (1996) 1707–1709.
[14] P.P. Neves, A.C. Doriguetto, V.R. Mastelaro, L.P. Lopes, Y.P. Mascarenhas, A. Michalowicz, J.A. Eiras, XAS and XRD structural characterization of lanthanum-modified $PbTiO_3$ ceramic materials, J. Phys. Chem. B 108 (2004) 14840.
[15] R. Tickoo, R.P. Tandon, N.C. Mehra, P.N. Kotru, Dielectric and ferroelectrics properties of lanthanum modified lead titanate ceramics, Mater. Sci. Eng. B 94 (2002) 1.
[16] D.A. Barrow, T.E. Petroff, R.P. Tandon, M. Sayer, Characterization of thick lead zirconate titanate films fabricated using a new sol–gel based process, J. Appl. Phys. 81 (1997) 876.
[17] R.K. Mishra, R.N.P. Choudhary, A.K. Thakur, Preparation and analysis of single-phase $Pb(Mn_{1/2}Nb_{1/2})O_3$,, J. Alloys Compd. 457 (1–2) (2008) 490–497.
[18] R.N.P. Shrabanee Sen, Choudhary phase transition in Sr modified $Pb(SnTi)O_3$ system, J. Alloys Compd. 457 (1–2) (2008) 417–421.
[19] R. Rai, B. Bihari, N.K. Singh, R.N.P. Choudhary, Structural and electrical properties of Sr-modified $Pb(NbMo)_3$ system, Phys. Status Solidi B: Basic Solid State Phys. 244 (3) (2007) 1118–1124.
[20] A. Taylor, X-Ray Metallography, Wiley, New York, 1961.
[21] G.K. Williamson, W.H. Hall, X-Ray line broadening from field aluminums and wolfram, Acta Metall. 1 (1953) 22–31.
[22] R.A. Young, The Rietveld Method International Union of Crystallography, Oxford University Press, New York, 1996.
[23] A.I. Kingon, B. Clark, Sintering of PZT ceramics: I. Atmosphere control, J. Am. Ceram. Soc. 66 (1982) 253–256.
[24] R. Ranjan, A.K. Singh, Ragini, D. Pandey, A comparison of the Cc and R3c space groups for the superlattice phase of $Pb(Zr_{0.52}Ti_{0.48})O_3$, Phys. Rev. B 71 (2005) 092101.
[25] Ragini, R. Ranjan, S.K. Mishra, D. Pandey, Room temperature structure of $Pb(Zr_xTi_{1-x})O_3$ around the morphotropic phase boundary region: a Rietveld study, J. Appl. Phys. 92 (2002) 3266.
[26] N. Sahu, S. Panigrahi, M. Kar, Structural study of Zr doped $PbTiO_3$ materials by employing Rietveld method. Adv. Powder Technol., in press, doi:10.1016/j.apt.2010.10.007.
[27] C. Sun, J. Wang, P. Hu, M.J. Kim, X. Xing, Effects of Al substitution on the spontaneous polarization and lattice dynamics of the $PbTi_{1-x}Al_xO_3$, Dalton Trans. 39 (2010) 5183–5186.